UNIVERSITY OF OKLAHOMA

GRADUATE COLLEGE

AN IMPLEMENTATION OF REAL TIME TESTBED OF COGNITIVE SWITCH FOR MULTI-USER FSOC LINK

A THESIS

SUBMITTED TO THE GRADUATE FACULTY

in partial fulfillment of the requirements for the

Degree of

MASTER OF SCIENCE IN ELECTRICAL AND COMPUTER ENGINEERING

By

KA HEI SAMUEL CHAN
Norman, Oklahoma
2021

Downloaded from SHAREOK. Persistent Handle URL: https://hdl.handle.net/11244/330724

TESTBED OF COGNITIVE SWITCH FOR MULTI-USER FSOC LINK

A THESIS APPROVED FOR THE
SCHOOL OF ELECTRICAL AND COMPUTER ENGINEERING

BY

Dr. Hazem H. Refai, Chair

Dr. Samuel Cheng

Dr. Choon Yik Tang

© Copyright by KA HEI SAMUEL CHAN 2021
All Rights Reserved.

Dedication

To my parents,

Stella and Gary,

my beloved brother, Kelvin,

my family

&

friends.

May freedom reign.

Acknowledgements

I would like to thank my advisor, *Dr. Hazem Refai*, for his patience, guidance, support, and opportunity to learn. Also, I appreciate for having the opportunity to undertake and further my studies within his research group at OU-Tulsa. I also would like to thank *Dr. Samuel Cheng* and *Dr. Choon Yik Tang* for agreeing to be part of my thesis committee. In addition, I would like to acknowledge the support and motivation from my colleagues during my research. Special thanks to Michelle Farabough for the editing of this thesis. Finally, I want to recognize the unlimited support of my family and friends.

Table of Contents

List of Figures ..... **vii**

List of Tables ..... **ix**

Abstract ..... **x**

Chapter 1: Introduction and Related Work **1**

Free-Space Optical Communication Technology *1*

Thesis Objective *6*

Chapter 2: Cognitive Switch **7**

Algorithm *7*

Similarity Measure 9

Number of User Detection 10

Runtime 10

Data Collection *12*

Equipment 12

System Measurement 15

Testbed Setup *18*

Experimental Results *20*

Threshold Determination 20

Number of User Detection 21

Runtime 23

Chapter 3: Signal Isolation by Independent Component Analysis **24**

Algorithm *24*

Testbed Setup *26*

Experimental Result *28*

Cross-correlation Validation 28

Chapter 4: Signal Isolation by Subtraction 30

Algorithm *30*

Testbed Setup *33*

Experimental Result *35*

Cross-correlation Validation 35

Conclusion and Future Work 37

References 38

Appendix A: Nomenclature 39

List of Figures

Figure 1. Simple, common layout of outdoor FSO design. Adapted from [4]. 2

Figure 2. Multipoint-to-point, adapted from [2]. 3

Figure 3. Fiber bundle serving as a receiving end. 3

Figure 4. Flowchart. 4

Figure 5. Cognitive switch flowchart. 8

Figure 6. Function generator. 12

Figure 7. Optical Transmitter. 13

Figure 8. Module board. 13

Figure 9. Transceiver. 13

Figure 10. Lens. 14

Figure 11. Optical switch. 14

Figure 12 Oscilloscope. 14

Figure 13. Photodiode. 14

Figure 14. Electrical v. optical at 100 Mpbs. 15

Figure 15. Electrical v. optical at 300 Mpbs. 15

Figure 16. Zoom of peaks. Electrical. 16

Figure 17. Zoom of troughs. Electrical. 16

Figure 18. Zoom of peaks. Optical. 16

Figure 19. Zoom of troughs. Optical. 16

Figure 20. Sharp transition on rise/fall time observed at 200 Mpbs. 17

Figure 21. Block diagram of the experimental setup with three users. 18

Figure 22. Actual cognitive switch testbed setup. 18

Figure 23. Threshold determination. 20

Figure 24. Histogram. Two identical users on State 1. 22

Figure 25. Histogram. Two identical users combined in State 2. 22

Figure 26. Histogram. A user on channel 1 and two users on channel 2 on State 1. 22

Figure 27. Block diagram of ICA. 24

Figure 28. Block diagram of the setup. 26

Figure 29. 50:50 optical coupler. 26

Figure 30. Cross-correlation v. data rate; PR = 0.78. 29

Figure 31. Cross-correlation v. data rate; PR = 1.55. 29

Figure 32. Cross-correlation v. data rate; PR = 3.08. 29

Figure 33. A separated channel receives a signal from one of two sources. Combined channel received a mixture from two sources. 30

Figure 34. Two users, different power, simulated. 32

Figure 35. Two users, equal power, simulated. 32

Figure 36. Block diagram of direct subtraction. 33

Figure 37. GUI of direct subtraction. 35

Figure 38. Cross-correlation v. data rate, PR = 0.46. 36

Figure 39. Cross-correlation v. data rate, PR = 3.81. 36

Figure 40. Cross-correlation v. data rate, PR = 5.39. 36

List of Tables

Table 1. Key features between FSO and RF technologies..... 2

Table 2. User power configuration. 19

Abstract

Free-space optical communication (FSOC) has been a popular alternative for radio frequency communication technology. Multiplicity and atmospheric turbulence are known to introduce fluctuations to FSOC link performance. Multiple-link FSOC performance can be simulated, implemented, and evaluated using a testbed. Experimental results indicate the feasibility of using a testbed for obtaining real-time signal comparison, user detection, and cognitive switching. This thesis presents a real-time, correlation-based methodology for signal comparison that can be used for detecting the number of communicating users and manipulating channels to isolate signals from mixed sources. The proposed methodology was experimentally validated using six approaches: 1) signal similarity by cosine similarity; 2) signal similarity by cross-correlation; 3) peak detection; 4) threshold determination; 5) real-time signal alignment; and 6) signal isolation.

Chapter 1: Introduction and Related Work

Free-Space Optical Communication Technology

The overall free-space optics (FSO) market is predicted to increase from USD 402 million in 2020 to USD 1977 million by 2025 [1]. This expansion reflects the technology's widespread acceptance as an alternative for oppressed radio frequency (RF) technology for outdoor wireless communication. Although most communication links are based on RF technology and suitable for a number of applications, network saturation has become more troublesome as the technology matures. Migration towards high data rate, high bandwidth, and secure connectivity are critical for future development of wireless communication. Free-space optics communication (FSOC) is an alternative for RF technology. This wireless communication technology utilizes optical spectrum of electromagnetic radiation, which is defined as in frequency range from 0.3 THz to 30 PHz and wavelength range from 1mm to 10nm [2]. FSOC has advantages over RF, including high density, high capacity, and high data rate. Table 1 compares key features of FSO and RF communication technology [3].

Table 1
FSO and RF Technology Key Features

Features	FSO	RF
Light Source	Photo Diode	Antenna
Receiver	Photo Diode	Antenna
Modulation	OOK, OFDM, QAM	ASK, PSK, QPSK, QAM
Licensed Spectrum	No	Yes (except Wi-Fi)
Link Coverage	>1000 km	>100 km
Bit Rate	40 Gbps	6 Gbps
Spectrum	Infrared/ visible light/ ultra-violet	Radio frequency
Line of Sight	Yes	No
Communication Topology	Bidirectional	Bidirectional
Security	High	Low
Latency	Low	High

FSO provides point-to-point communication, meaning that light travels though free-space typically in a straight line. Line of sight is required, hence, providing a secured link. To establish such a point-to-point link, a pair of transceivers are used for emitting and receiving signals. A simple, common flow diagram of an outdoor FSO design modeled with a propagation channel is shown in Fig. 1 [4]. This design indicates that a pair of lenses are used to emit and to receive a signal.

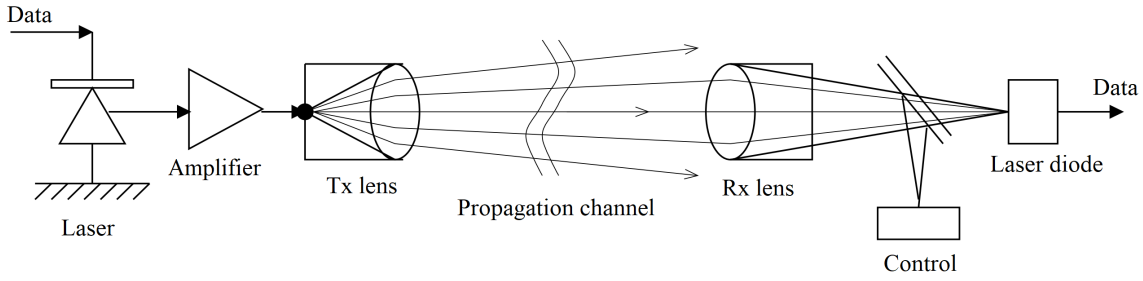

Figure 1. Simple, common layout of outdoor FSO design. Adapted from [4].

FSO also provides multipoint-to-point and point-to-multipoint communication [2], which require special transceivers. Consider the design of a smart city that utilizes infrastructure-to-vehicle (V2X) as a method of outdoor, medium-range optical wireless communication (OWC), as shown in Fig. 2 [2]. Given that a bundle of laser diodes is used in the design as the method of receivers instead of camera, the system can be represented in the flowchart [5] shown in Fig. 3. The fiber bundle shown in Fig. 2b can serve as the bundle of laser diodes used in the traffic light [5]. Design can be simulated and tested by the experimental setup shown in Fig. 3 [5]. The reported study demonstrated a testbed that evaluated multipoint-to-point OWC performance using a fiber bundle as a single receiving node and using lasers with various wavelengths, data rates, and powers as transmitting nodes.

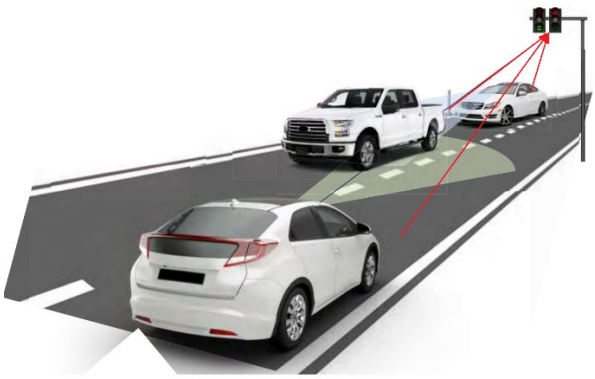

Figure 2. Multipoint-to-point, adapted from [2].

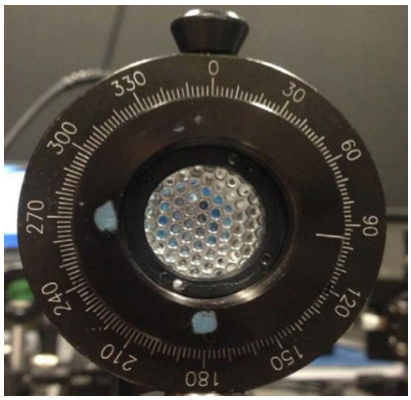

Figure 3. Fiber bundle serving as a receiving end.

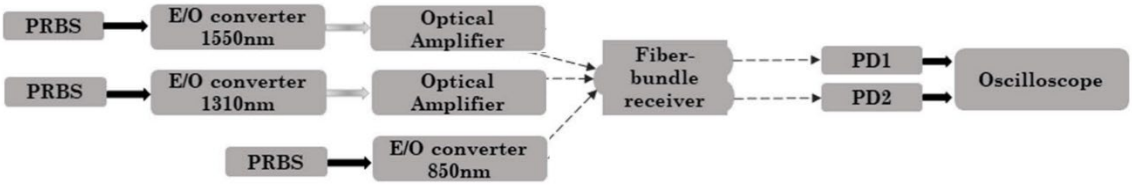

Figure 4. Flowchart.

In FSOC, several modulation schemes have been exploited, of which intensity modulation and direction detection (IM/DD) has proven practical and is widely used [6]. In this technique, source optical power output is varied based on various modulations.

Basic optical modulation on-off keying (OOK) is an amplitude-shift keying (ASK) modulation that carries data as the presence or absence of the carrier. In this modulation, a "one" bit is coded as high, and a "zero" bit is coded as low. This procedure is based on its bit rate, defined as $R_b = \frac{1}{T_b}$, where T_b is the bit duration.

However, both point-to-point and multipoint-to-multipoint OWC have limitations and challenges. FSO technology utilizes atmosphere as travel media. Channel can be modeled with propagation in space and time for a given weather and geographical location. For long-range FSOC, beam divergence is a factor of a stable communication link. Notably, beam changes its property—mainly traveling angle and speed— when traveling though air—due to light diffraction from change in air temperature, humidity, and weather of different geographical locations. The precondition of a successful, stable link is that the beam arrives at the receiver aperture [2]. Link reliability depends on low atmospherics turbulence (e.g., no rain or clouds). Beam divergence is inversely proportional to the aperture diameter and directly proportional to beam wavelength. Hence, an optical beam is narrower when compared to an RF carrier. FSOC requires stable line-of-sight (LOS) communication between transceivers. Atmospheric

fluctuations may degrade communication performance (e.g., the relationship between a fixed receiving lens with small focal radius and the constantly changing air temperature such that light is bent and no longer travels in a straight line [7]).

Bearing in mind multipoint-to-multipoint OWC with several users, one might consider how a fiber bundle serving as a single receiving node would isolate multiple signals at a given time? Likewise, how would each signal isolate from a mixed source? Multiple access techniques in a high-speed, free-space optical communication have been investigated to address such questions. Authors in [5] used Independent Component Analysis (ICA) as an unsupervised blind source separation (BSS) and observed at least 0.80 cross-correlation coefficient when reconstructing source signals from BSS and atmospheric turbulence. As an alternative to ICA, this thesis investigates the performance of real-time implementation.

Thesis Objective

This thesis is written with the objectives of characterizing a testbed for FSOC. The focus is limited to real-time, cognitive switching and multi-user signal isolation

- to establish a real-time testbed that combines similar signals and
- to isolate multiple users from a single channel.

The balance of this thesis is structured, as follows.

- Chapter 1 introduces the background and related work of FSOC and cognitive switch.
- Chapter 2 describes the algorithms used for the cognitive switch and how real-time signal comparison is used in the algorithm.
- Chapter 3 focuses on the BSS algorithm of ICA.
- Chapter 4 discusses the signal separation algorithm of direct subtraction.

Chapter 2: Cognitive Switch Algorithm

Various states of optical switches were determined by manipulating user number in coherent channel, cosine similarity, cross-correlation, and threshold determination. Calculations were completed on the PC. Fig. 4 provides a system flowchart that describes state determination. Although the optical switch used in the experiments has an input and two outputs, only a single output can be used at any given time. Switch's output can be controlled by the on-board logic board when triggered by a transistor–transistor logic (TTL) signal. First, number of channels being used is determined, as only two channels can be compared at once. Hence, the number of channels being used must be greater or equal to two. Second, the system synchronizes all switches, setting them to State 1 (i.e., first output of the switch), which enables State 1 loop to commence. Next, the oscilloscope samples the corresponding channel for each user on State 1. Finally, the number of users is calculated. Given a single or fixed number of users is detected on each channel, processing will compare similarity with another single-user channel. If both share high similarity (i.e., higher thresholds), the channel will be switched to State 2 wherein the switch's second output will be combined via an optical combiner. In addition, signals will be combined with an optical combiner characterized by equal gain. In State 2 the system will wait for a period—two seconds in this setup—to protect the switch from high speed and frequent switching. Number of users in State 2 can then be calculated. Given that this number has increased, the system will switch back to State 1; otherwise, the system will continue in a State 2 loop.

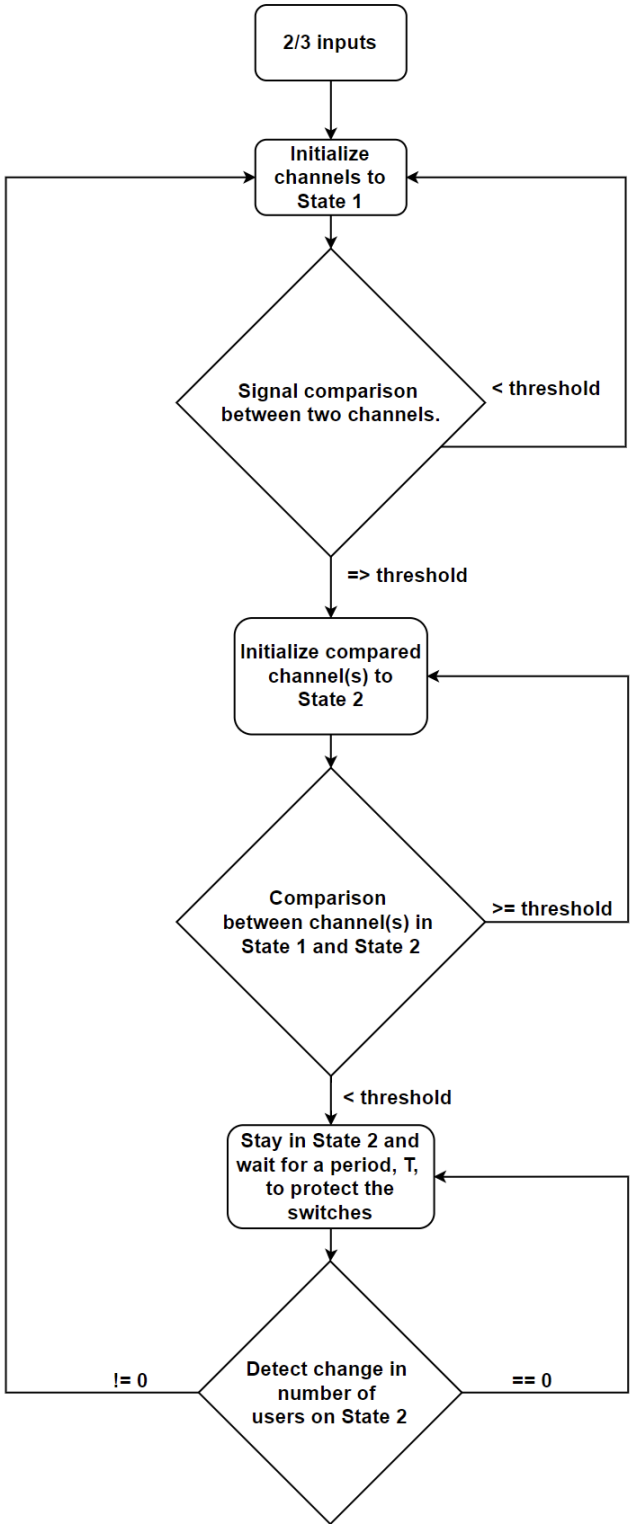

Figure 5. Cognitive switch flowchart.

Similarity Measure

To compare signal similarity, cosine similarity and cross-correlation between two input vectors are calculated.

a) Cosine similarity between two vectors A and B is defined as follows:

$$\cos(\theta) = \frac{A \cdot B}{|A||B|}, where\ \cos(\theta)\,\epsilon(0,1)$$

b) The return of a cross-correlation operation between two normalized arrays, A and B, is an array of it convolving two input arrays. Maximum cross-correlation coefficient between A and B indicates the most similar to each other, wherein lag is calculated. This is defined as follows:

$$\max(R_{AB}) = \max\,(E[AB^T]), where\ \max(R_{A_B})\epsilon(-1,1)$$

c) Regarding threshold determination, the system first initializes State 1 in which each input signal has its own oscilloscope channel. Given that the signals are similar (i.e., above threshold), they will be combined into State 2. Hence, similarity thresholds are needed for determining when the system switches between states.

Moreover, simulated input signals become noisy having processed through the system of function generators, optical transceivers, lenses, free space, optical switches, and photodiodes. This noise addition implies a real-life scenario; therefore, thresholds vary in different scenarios and can be determined by experimenting with cognitive switches, incremental thresholds, and least error rate thereof.

Error rate can be determined in two ways based on the concept of confusion matrix. First, the algorithm counts the number of times the switch fails to change when it

should (i.e., false negative). Second, it counts the number of times the switch changes when it should not (i.e., false positive).

Running a fixed number of trials and counting the number of errors for system switching provides a usable error rate. Thresholds can then be set as the experiment increments at the point at which the least error rate is one step before rising above zero. When determining one threshold, other parameters should be held constant so that when cross-correlation is tested, cosine similarity can be ignored, and vice versa.

Number of User Detection

Each data acquisition is transformed into a histogram. Peak counting algorithm takes the derivative of the histogram function and seeks local maxima [8]. For smoothing the algorithm outcome, a threshold can be set to eliminate fluctuation from noisy real-time sampling. In this way, the outcome is steady as opposed to bouncing within a range. For simplicity, thresholds of each histogram are set manually according to input signal fluctuation. Validation between outcome and source is achieved by manually matching input peaks.

Chapter 2 of this thesis is primarily concerned with counting number of peaks with regard to the peak counting algorithm. Relative peak positions are considered, and algorithm details are further explained in Chapter 4.

Runtime

Considering that only two input vectors will be taken in the same execution loop, given the number of inputs is greater than two, total execution time is expected to be multiplied with the number of combinations, where number of combinations, n, is defined as follows:

$$n = \binom{k}{2}, where\ k\ is\ the\ numebr\ of\ inputs.$$

A complete execution loop for this testbed requires a sequence of data fetching, array comparison, and outputting. Array comparison runtime should be further investigated, as it represents the number of execution loops for a given time period. Essentially, the more input, the longer the runtime and slower the actual sampling rate.

Data Collection

Real-time continuous collection was maintained on all four channels. Each acquisition consisted of 10,000 time-series data points at a sampling rate of 10 GHz on each channel. Each acquisition was then passed to a PC with a 1.90-GHz Intel Core i7-8650U processor via ethernet or USBTMC for data processing with a custom LabVIEW program.

Equipment

SIGLENT's SDG6032X dual-channel pulse/arbitrary waveform generators produce three pseudo-random bit sequences (PRBS) (e.g., PRBS-3, PRBS-5, or PRBS-7, etc.) with corresponding bit sequence length at data rates that vary from 10 to 300 Mbps. Each function generator has two output terminals, which can either be synchronized or asynchronized to each other. Both function generators can be controlled by a PC with a LabVIEW program. Signals are set to on-off keying (OOK) with intensity modulation / direct detection (IM/DD).



Figure 6. Function generator.

User 1 obtained optical PRBS with wavelength 1550 nm from a channel of function generator 1 (See Fig. 5), which was driven by an electrical-to-optical converter (E/O), Thorlabs MX10B high-speed digital reference optical transmitter, C-band laser, as shown

in Fig 6. The transmitter has built-in embedded optical attenuator for variable transmitting power. User 2 and 3 obtained PRBS from channel 1 and 2 of function generator 2, which were driven by two optical module transceivers (e.g., E/O, small form-factor pluggable (SFP) with wavelength 1310 nm and 1550 nm, respectively), as illustrated in Fig. 7. Two Hitech Global SMA-to-SFP/SFP+ conversion module boards (See Fig. 8) were used with Cisco transceiver modules of 1310 nm and 1550 nm (See Fig. 9). The transceivers have fixed powers, with external optical attenuators (Thorlabs VOA50-FC) used for adjusting transmission power.

.



Figure 7. Optical Transmitter.

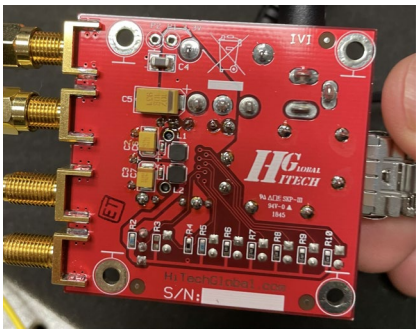

Figure 8. Module board.



Figure 9. Transceiver.

Signals traveled through Air-Spaced Doublet Collimator Packages (i.e., lenses) with corresponding wavelengths (Fig. 10), and entered independent switches (Thorlabs OSW12-1310E), as depicted in Fig. 11, which were controlled by the algorithm described in Chapter 3.1.



Figure 10. Lens.

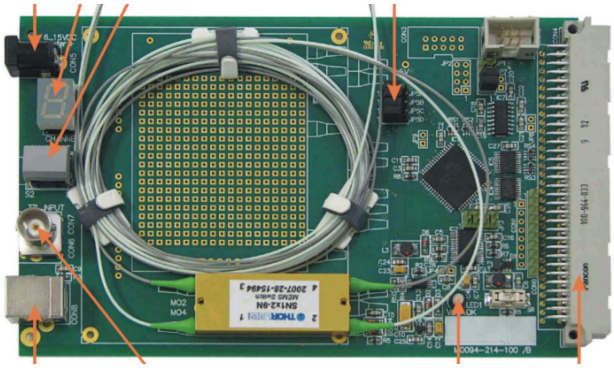

Figure 11. Optical switch.

After passing through the switches and before entering separated channels of an oscilloscope (WavePro 254HD-MS), shown in Fig. 12, the signals entered independent photodiodes (Thorlabs DET08CFC) or optical-to-electrical converter (O/E), depicted in Fig. 13, and were converted from optical signals to electrical signals. The oscilloscope was set to maximum sampling rate of 10 Gsample/s per channel for all four channels.



Figure 12 Oscilloscope.

.



Figure 13. Photodiode.

The oscilloscope was linked by a 10/100/1000BaseT ethernet interface or USBTMC over USB 3.1 Gen 1 interface for communicating to the PC with a custom LabVIEW program for data collection, visualization, analysis, and control. Finally, Arduinos were used to receive commands from the PC and to control the switches.

System Measurement

- Correlation between electrical input and optical output

For validating the output of the algorithms in this thesis, results can be compared to the source by calculating correlation. In particular, it is necessary to know the comparison source, which can be determined by knowing how an electrical source correlates with its optical output. The cross-correlation coefficients between electrical source from the function generator and optical signal emitted from the transceiver are calculated at approximately 0.70 to 0.73 at different data rates. Consider finding the coefficient, as detailed in chapter 2. Similarity Measure and lag between two inputs is included in the calculation, so that the asynchronization between them can be ignored.

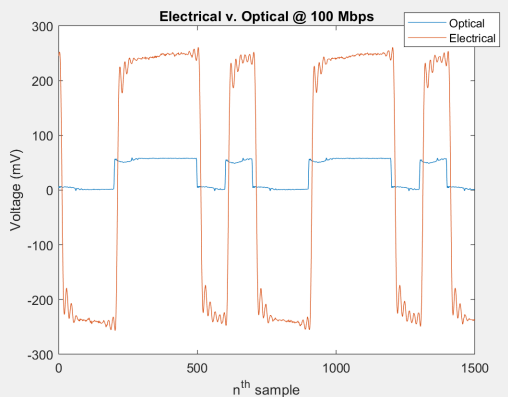

Figure 14. Electrical v. optical at 100 Mpbs.
(a)

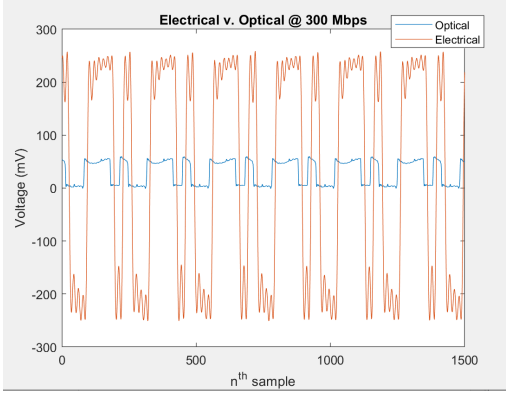

Figure 15. Electrical v. optical at 300 Mpbs.
(b)

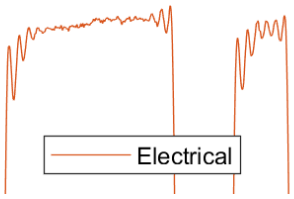

Figure 16. Zoom of peaks. Electrical.

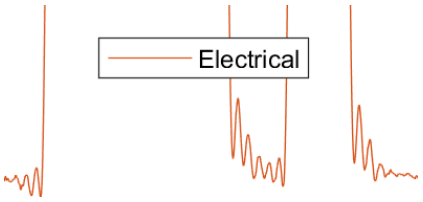

Figure 17. Zoom of troughs. Electrical.

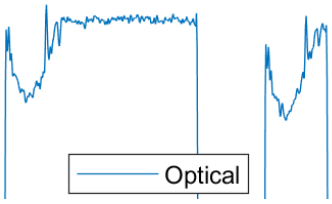

Figure 18. Zoom of peaks. Optical.

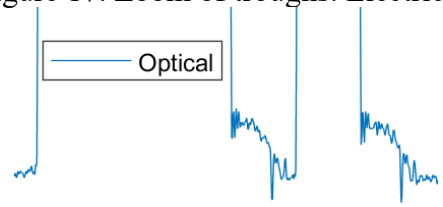

Figure 19. Zoom of troughs. Optical.

Figures 16 and 17 show that the electrical signal was undershooting at the rising edge, overshooting at the falling edge, and damping to the target voltage. Figures 18 and 19 show that optical signal was undershooting at the rising edge and overshooting at the falling edge. This systematic error caused correlation coefficients depicted in this section.

Consequently, only the optical signal can be used as a reference in this thesis.

- Switch rise/fall time

The rise/fall time of the switch must be determined to serve as one of the variables for an FSOC testbed. Since data loss may occur when the switch is flipped from one state to another, the rise/fall times of the electrical signals sent from the function generators were set to their minimum (1.0 ns) and their maximum to facilitate further investigation. For example, maximum rise/fall times are 8.0 ns, 4.1 ns, and 2.8ns at bit rate 100 Mbps, 200 Mbps, and 300 Mbps, respectively.

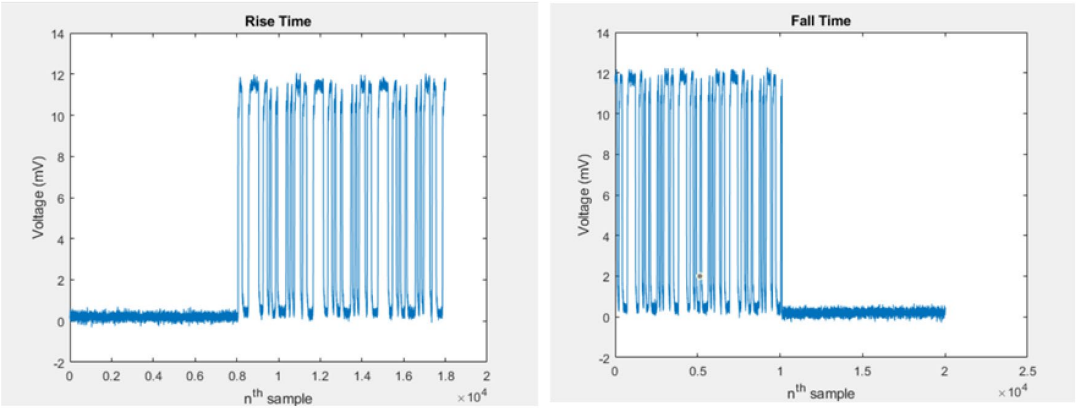

Figure 20. Sharp transition on rise/fall time observed at 200 Mpbs.

Fig. 20 shows that the switch flipped instantly without a blunt transition.

Testbed Setup

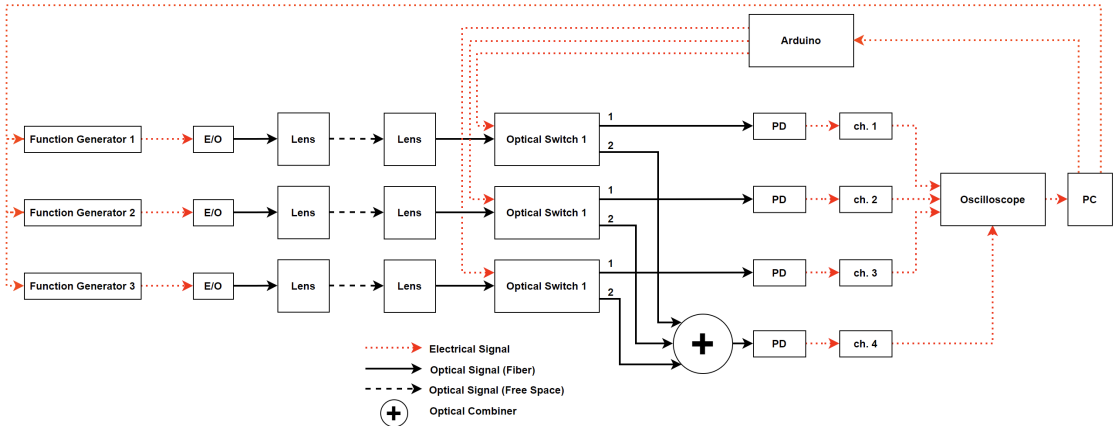

Figure 21. Block diagram of the experimental setup with three users.

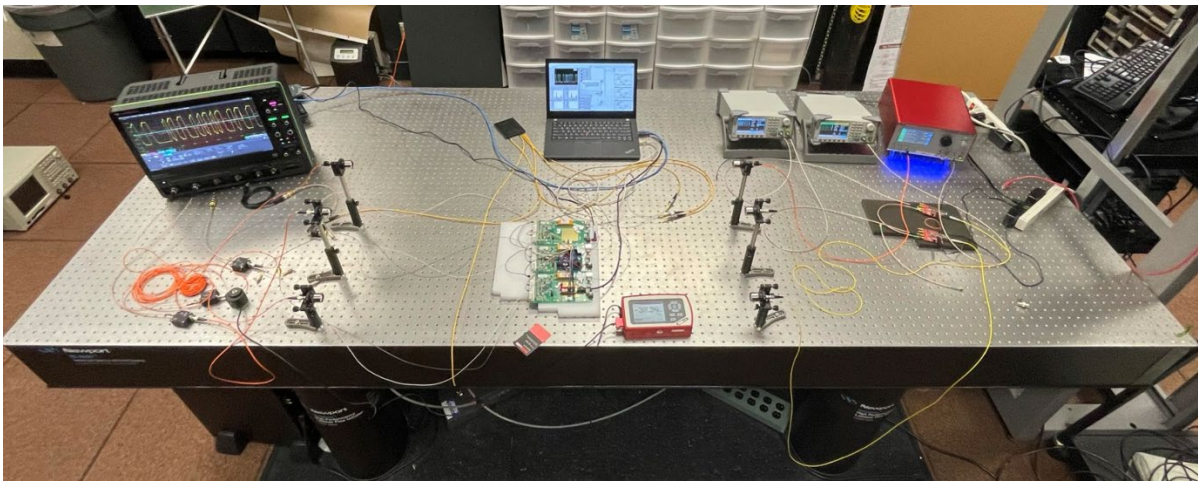

Figure 22. Actual cognitive switch testbed setup.

Figure 21 shows the block diagram of the setup for three users. Red dotted lines, black solid lines, and black dashed lines represent electrical links, fiber optical links, and free-space optical links, respectively.

Transmitted powers were set accordingly for a controlled case and an after-switch case. For the controlled case, signals were transmitted through lenses 2.85 dBm, 2.77 dBm, and 2.65 dBm for Tx user 1, 2, and 3, respectively. Received powers were 2.35 dBm, 2.30 dBm, and 2.19 dBm at the receiving lenses. For the after-switch case, signals

were transmitted through lenses and an optical switch. Received powers were -1.02 dBm, -1.18 dBm, and -1.30 dBm at the optical switches. Due to hardware limitation, signals were set 2 dBm apart to represent an after-switch case, as 2.85 dBm, -0.88 dBm, and -1.19 dBm for Tx user 1, 2, and 3, respectively. Received powers were 2.35 dBm, -0.31 dBm, and -1.62 dBm at the receiving lenses. Received powers were -1.02 dBm, -3.08 dBm, and -5.12 dBm at the optical switches.

Table 2

User Power Configuration

User 1,2,3	controlled (dBm)	After-switch (dBm)
Power at TX lenses	2.85, 2.77, 2.65	2.85, -0.88, -1.19
Power at RX lenses	2.35, 2.30, 2.19	2.35, -0.31, -1.62
Power at switches	N/A	-1.02, -3.08, -5.12

Transmitted signals traveled through air separated by 2 m, the ambient air was measured as 23.0 °C, and 27.3 % relative humidity. Signals were received by lenses, and then channeled via 1-by-2 Thorlabs OSW12-1310E-SP2 optical switches into State 1 or State 2. State 1 signals were transformed into electrical signals via photodiodes, and then input into individual, separated channels of an oscilloscope for further analysis.

State 2 signals were combined with equal gain by an optical combiner (e.g., Newport/s F-CPL_B14350), transformed into electrical signals, and then input into a channel of the oscilloscope. A sample was collected via the oscilloscope and transferred to a PC. The system was controlled by a custom program written in LabVIEW for

analyzing input signals and outputting state values to Arduino, and then triggering optical switches. The PC controlled function generators for automation.

Experimental Results

Threshold Determination

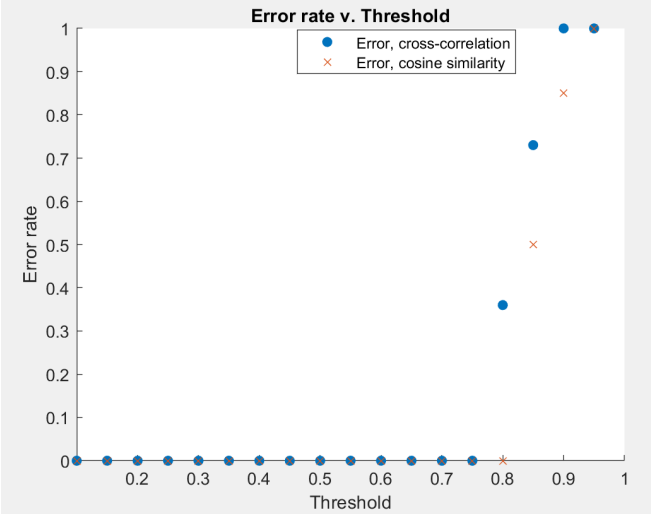

Figure 23. Threshold determination.

When two identical synchronized signals were entered into the system, false negative rate was at threshold 0.8 for cross-correlation and 0.85 for cosine similarity. Threshold increased by 0.05 for each increment (See Fig. 23).

The system remained on State 1 at all threshold levels when two signals were input. There was a zero false positive rate.

Consequently, thresholds 0.75 and 0.80 were tested for cross-correlation and cosine similarity, respectively. These variables were selected, as the next increments resulted in failure. The system switched from State 1 to State 2 when both cosine and cross correlation coefficients were above thresholds.

Number of User Detection

The histogram indicated the correct number of users on a given channel; each channel input was characterized by a given number of users. The system was tested when single, dual, and triple users coalesced by way of an optical combiner before passing through a channel. The algorithm displayed the corresponding number of peaks after assigning signal lows to “zeros” and signal highs to “ones.” A threshold was manually set based on signal fluctuation for each peak count in the histogram.

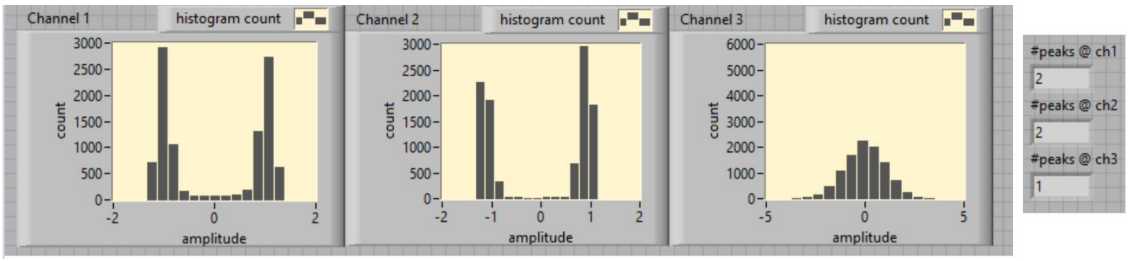

Figure 24. Histogram. Two identical users on State 1.

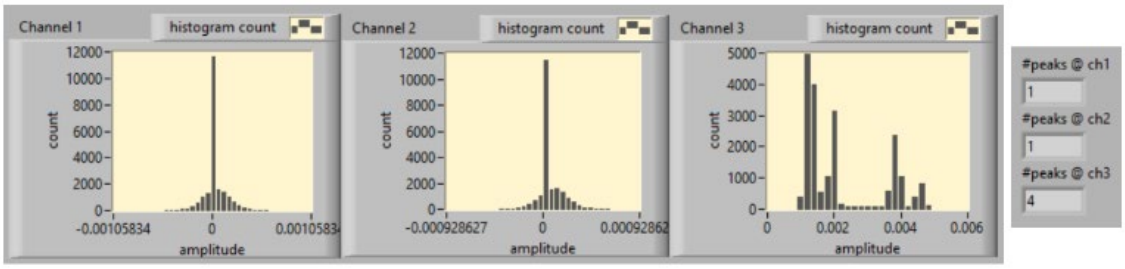

Figure 25. Histogram. Two identical users combined in State 2.

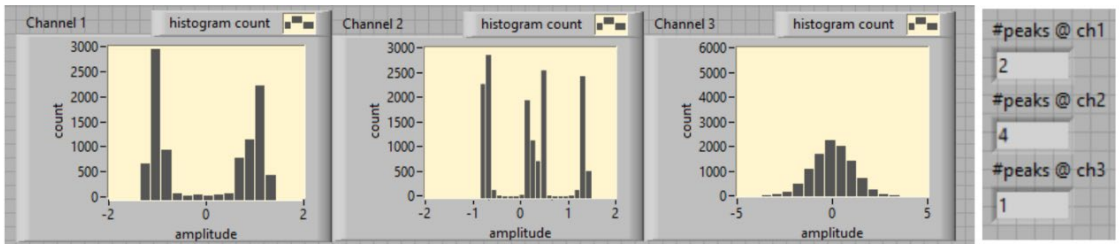

Figure 26. Histogram. A user on channel 1 and two users on channel 2 on State 1.

In Fig. 24, the histogams showed two identical sychronized users on State 1. Since channel 3 was in open channel, so it was showing Gaussian noise from the environment. The graphical user interface (GUI) correctly showed the number of peak count.

Histogamsdepicted in Fig. 25 reported two identical sychronized users on State 2. Systematic error was introduced, and received power from two receiving lenses was not identical. Peak divergence leveraged the algorithm provided in Chapter 4, so that four peaks were counted. In State 2 was characterized byState 1 channels that were blocked by

the switching mechanism for each switch. Little to no amount of light was able to leak into State 1. Consequently, a significant number of zeros were displayed in the Channel 1 and Channel 2 histogram. The GUI correctly showed the peak count.

Histograms depicted in Fig. 26 reported two user types in State 2: one type on channel 1 and two users combined on channel 2. The system stayed on State 1 accordingly. The GUI correctly showed peak count.

Results indicated that the "number of users" detection algorithm performed as expected, showing the correct peak count on different switch States.

Runtime

Two methods (e.g., USBTMC and ethernet) tested the connection speed between the oscilloscope and the PC. Average time per iteration were 103 ms and 181 ms for USBTMC and ethernet, respectively. Due to hardware limitations, we were only able to increase number of users only from two to three. Average time per iteration remained stable when number of users increased from two to three. There was no observable increase in runtime given an increase in the number of users.

Chapter 3: Signal Isolation by Independent Component Analysis Algorithm

ICA is a BSS technique widely used to separate multivariate signals into additive subcomponents [8]. Two assumptions are made: 1) subcomponents are statistically independent of each other and 2) they are non-Gaussian distributed.

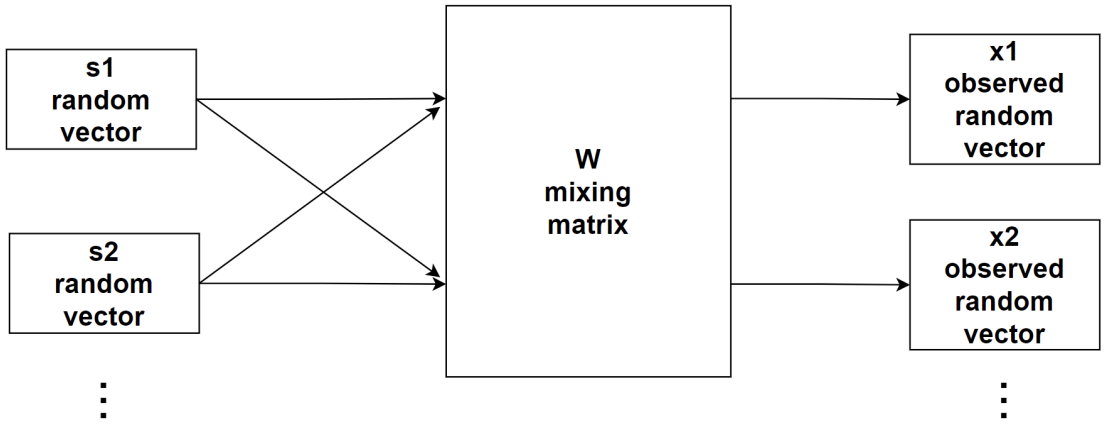

Figure 27. Block diagram of ICA.

We considered m number of observed signals as random variables represented by vector $\vec{\boldsymbol{x}}$, where $\vec{\boldsymbol{x}} = [\boldsymbol{x_1}, \boldsymbol{x_2}, \boldsymbol{x_3}, \ldots \boldsymbol{x_m}]^{\boldsymbol{T}}$. n number of hidden sources were also considered random variable $\vec{\boldsymbol{s}}$, where $\vec{\boldsymbol{s}} = [\boldsymbol{s_1}, \boldsymbol{s_2}, \boldsymbol{s_3}, \ldots \boldsymbol{s_n}]^{\boldsymbol{T}}$. ICA transformed vector $\vec{\boldsymbol{x}}$ into a vector of maximally independent components s, using linear mixing matrix $\overrightarrow{\boldsymbol{W}}$. The ICA model can be represented as follows: $\vec{\boldsymbol{x}} = \boldsymbol{W}\vec{\boldsymbol{s}}$ or, to find hidden sources $\vec{\boldsymbol{s}}$, the model can be represented as $\vec{\boldsymbol{s}} = \boldsymbol{W}^{-1}\vec{\boldsymbol{x}}$ [5]. For simplicity, number of observed vectors is equal to number of hidden sources (i.e., m = n, and $\overrightarrow{\boldsymbol{W}}$ is non-singular so that $\vec{\boldsymbol{s}}$ has a solution.

Since ICA generates a new set of statistically independent time series arrays, the algorithm can be used during setup to isolate mixed signals from the original time series arrays that are statiscally dependent on one another.

The FastICA algorithm is more efficient,, as it first calculates negentropy J (i.e., non-Gaussiantiy of a time series) as follows [9]:

$$J(y_i) = \left[E\left(G(y_i)\right) - E(v)\right]^2, for\ i = 1, 2, \dots, n$$

where n is the number of independent components; y_i is independent components; G is any non-quadratic function; and v is a Gaussian variable with zero mean and unit variance. FastICA then adjusts a separating matrix for combining each independent component y_i into X_t to maximize negentropy, which measures nongaussianity of the time series input arrays, so that components are statistically independent.

Before running ICA, channels were aligned by determining lags from calculating cross-correlation. Zero padding misalignment can be used for alignment.

Validation is accomplished by comparing outcome similarity of this algorithm (i.e., difference between the subtrahend and the minuend to an external signal from a separated source).

Testbed Setup

The equipment used for this testbed setup were similar to those used in 3.2.2. The exception was an optical mixer used to present $\overrightarrow{\boldsymbol{W}}$ (i.e., the mixing matrix). Due to hardware limitations and simplification, only two sets of signals were computed by ICA for results reported in this chapter.

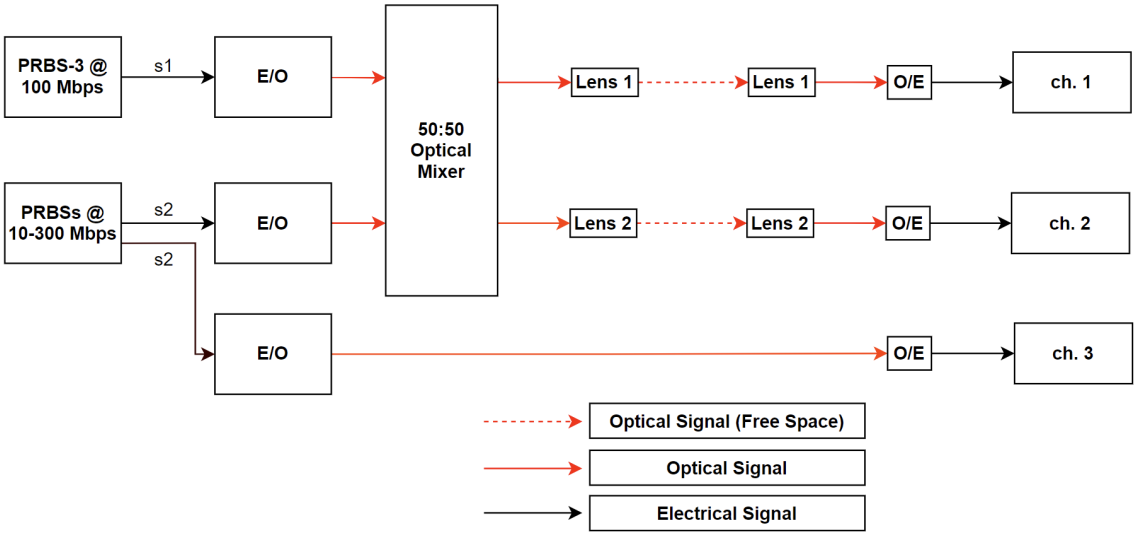

Figure 28. Block diagram of the setup.



Figure 29. 50:50 optical coupler.

TN1550R5A2 50:50 optical coupler from Thorlabs was selected for testing. To simulate actual communication, a function generator produced a fixed PRBS-3 at 100

Mbps as a controlled variable. Another function generator produced varying PRBS starting PRBS-3 to PRBS-15 at bit rates varying from 10 Mbps to 300 Mbps. The generator also output the same signal to a separated channel for validation.

Hardware limitation and simplification limited testing to only one constant signal and one variable signal. Power of s1 was fixed at 1.90 dBm measured at the E/O before entering the 50:50 optical mixer; s2 powerwas 3 dBm apart for observing variable power outcomes4.89 dBm, 1.91 dBm, and -1.09 dBm measured at the E/O before entering the optical mixer. No power measurement was needed at the lenses before entering O/E, since signals were varied by the mixer and power level would be shown directly in the oscilloscope.

To validate whether or not isolated signals were similar to the sources, similarity between isolated signals and the sources were compared, as was in 2.1.1. Validation was measured using bit rates, PRBS patterns, and power difference. An identical copy of s2 was entered into a seperated osscilopescope channel whereinthe copy compared algorithm outcome to the source by justifying the similarity between them. Maximum coeffeicent was recorded as each power and PRBS set. Each set ran for a fixed period of time to avoid neglecting any PRBS pattern for any sampling window.

Experimental Result

Cross-correlation Validation

The effectiveness of data rates, signal power, and FastICA algorithm were investigated. The experimental setup included a 3 dB difference in optical power of signal B; signal A was set at a constant PRBS-3 at 100 Mbps. Power ratio between signals A and B is defined, as follows:

$$PR = 10 \log\left(\frac{P_{s2}}{P_{s1}}\right) \, dB$$

Figures 30 through 32 show that all experimental sets reached at least 0.89 cross-correlation coefficient among all power ratios, data rates, and PRBSs. Mostly, the variables fluctuated between 0.89 and 0.92. Surprisingly, when signals A and B were set to PRBS-3, cross-correlation coefficient was higher than other bit sequence patterns.



Figure 30. Cross-correlation v. data rate; PR = 0.78.



Figure 31. Cross-correlation v. data rate; PR = 1.55.



Figure 32. Cross-correlation v. data rate; PR = 3.08.

Chapter 4: Signal Isolation by Subtraction Algorithm

Considering a scenario in which a channel receives a mixed signal from two sources, another channel will receive part of a signal from one of two sources. In this scenario, direct subtraction can be used to isolate source signal from a mixture.

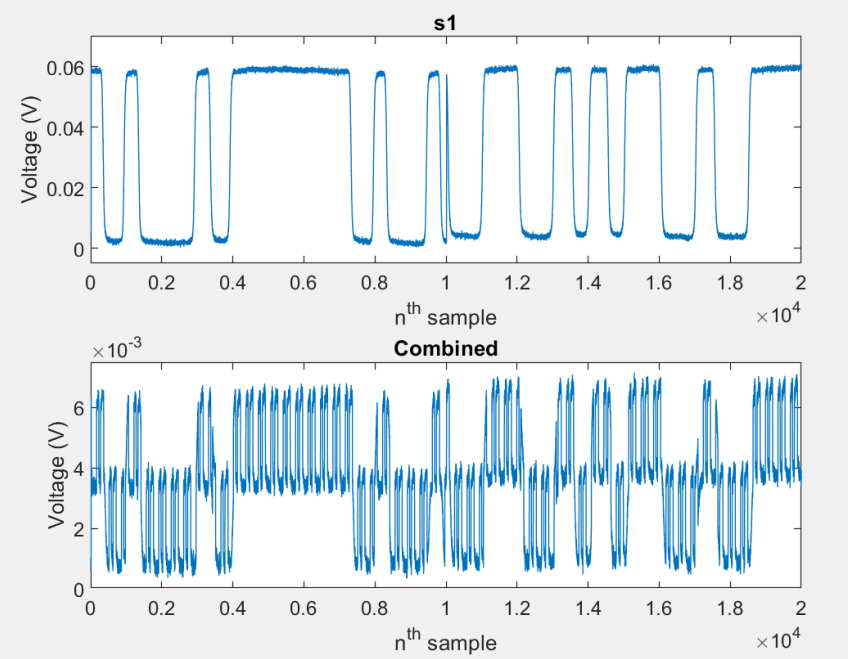

Figure 33. A separated channel receives a signal from one of two sources. Combined channel received a mixture from two sources.

After data are fetched from each channel, they are normalized and aligned. To align two input arrays and eliminate experimental error from actual setup, calculating cross-correlation is used for returning the number data points from which the arrays are lagging or advancing each other. Data are also transformed into histograms. Peak count is necessary for each histogram to determine threshold for smoothing the outcome from the peak counting algorithm. Subtrahend (i.e., the number subtracting) and minuend (i.e., the number being subtracted) must be assigned to the two arrays for differing and isolating

the signals. This decision is based on the peak counting algorithm. The difference between two arrays will be the isolated signal.

Besides aligning the lags of two input signals, the signal power range difference must be accounted for. Hence, the signals must be rescaled for direct subtraction. In the algorithm under test, input signal powers are rescaled based on histogram results.

Figure 34 shows the results of two ideal users with different powers passing through free-space represented by a white Gaussian noise channel. Assuming each user has equal probability for outputting highs and lows, User 1 indicates lower power. Given an acquisition histogram, peak 1 indicates that both users had low output; peak 2 indicates that only User 1 output high. Peak 3 indicates User 2 output high; and peak 4 indicates both users output high. Note that the distance between peak 1 and 2 should be equal to the distance between peak 3 and 4, since combining on-off-keying (OOK) optical signals behave as linear summation. Therefore peak 1 indicates exclusively low power for all users, and peak 2 indicates that User 1 power is high. Peak 3 indicates User 2 power is high, and peak 4 indicates a sum of all users.

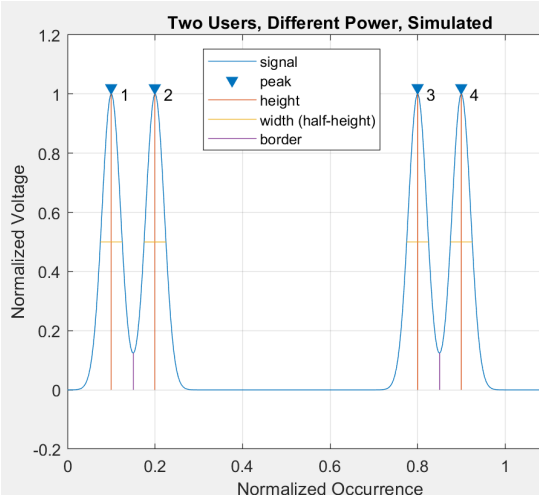

Figure 34. Two users, different power, simulated.

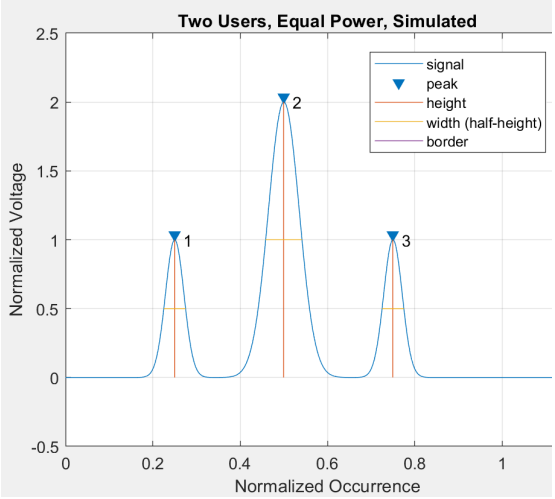

Figure 35. Two users, equal power, simulated.

Figure 35 informs that two users share same output power. Distance between the adjacent peaks should be equal. Therefore, the peak 1 denotes that all users have low power, and peak 2 denotes one user's power is high and the other is low. Peak 3 denotes high power from both users. As such, the distance projected on the occurrence axis between peaks can be used to indicate each user. Assumptions were made in the proposed algorithm. First, for simplification, only two pairs of lenses were used. Second, powers remained constant in each acquisition. Before running ICA, channels were aligned by determining lags from calculating cross-correlation. Zero padding misalignment determined alignment.

Like in Chapter 3, validation was possible by comparing algorithm outcome similarities (i.e., the difference between subtrahend and minuend for an external signal from a separated source).

Testbed Setup

The equipment used for the setup reported in this thesis are similar to those detailed in Chapter 3. The only exception is that a combined optical was used for mixing the split signal. Fig. 36. Shows that function generator 1, namely s1, output constant PRBS-3 at 100 Mbps. Function generator 2, namely s2, output varying PRBS at different bit rates ranging from 10 Mbps to 300 Mbps. Both electrical signals were transformed into optical signals by E/O. Optical signal s1 was split into lens 1 and an optical combiner using a 50:50 optical splitter. s2 was fed directly into the optical combiner. The mixture (i.e., half s1 and half s2) were entered into lens 2 after being mixed by the optical combiner. Therefore, channel 1 of the oscilloscope was expected to receive half of s1, while channel 2 received the mixture.

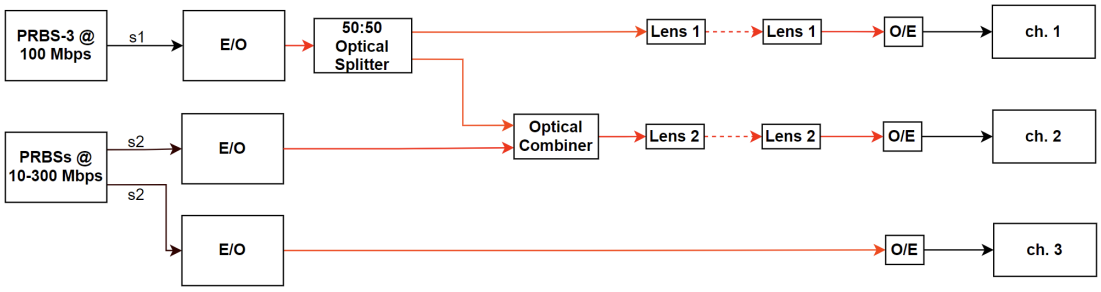

Figure 36. Block diagram of direct subtraction.

As aforementioned, hardware limitations and simplification permitted the use of only one constant signal and one variable signal in the testbed setup. Power of s1 was fixed at 2.30 dBm, which was measured at the E/O before entering the 50:50 optical splitter. Power of s2 was set 3 dBm apart (i.e., -0.68 dBm, 2.26 dBm, and 5.28 dBm measured at the E/O before entering the optical combiner) for observing variable power

outcomes., Before O/E, channel 1measured powers were -5.30 dBm, -4.21 dBm, -3.70 dBm, and channel 2 were -4.84 dBm, -0.40 dBm, and 1.69 dBm.

Like validation in Chapter 3, bit rate, PRBS pattern, and power difference served as variables. An identical copy of s2 was entered into a seperated osscilopescope channel wherein it is compared with algorithm outcome by justifying the similarity of results. Maximum coeffeicent was logged as each power, and PRBS was set. Each set operated for a fixed period of time to avoid neglecting any sampling window PRBS patterns.

Experimental Result

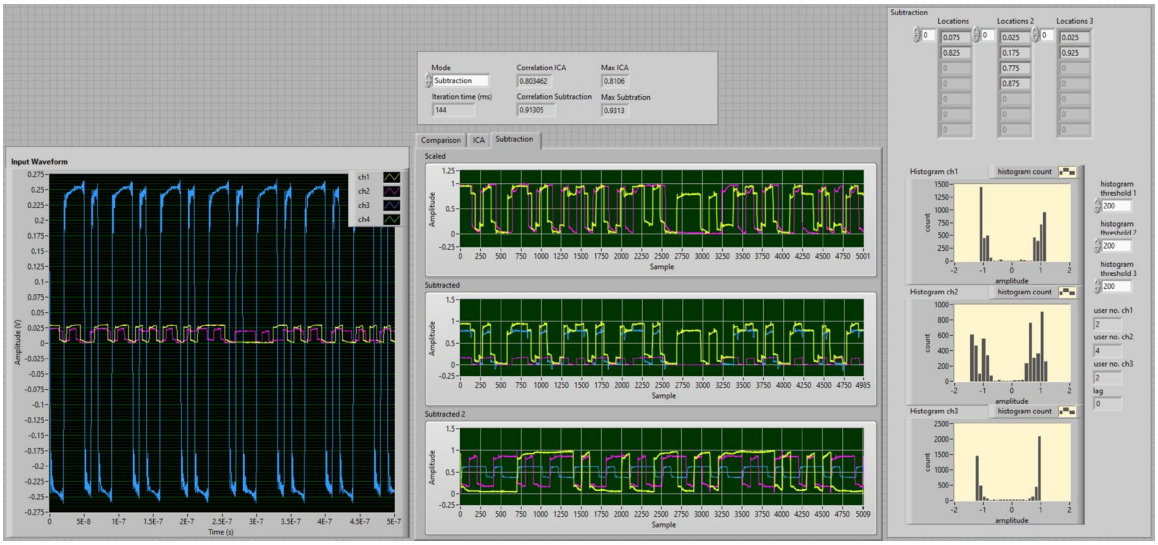

Figure 37. GUI of direct subtraction.

Cross-correlation Validation

The effectiveness of data rates, signal power, and the direct subtraction algorithm were investigated. Variables were identical to experiments reported in Chapter 4. Signal B optical power difference was 3 dB apart, and signal A was constant with PRBS-3 at 100 Mbps.

Figures 38 through 40 show that all experimental sets reached at least 0.77 cross-correlation coefficient among all power ratios, data rates, and PRBSs. Generally, fluctuations were between 0.89 to 0.97, 0.82 to 0.91, and 0.77 to 0.84 for PR 0.46, 3.81, and 5,39 respectively. When signal B was set to be PRBS-3, which was the same as signal A, cross-correlation coefficient proved higher than other bit sequence patterns.

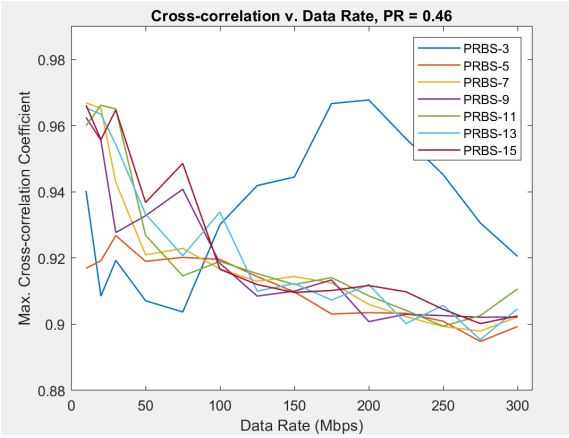

Figure 38. Cross-correlation v. data rate, PR = 0.46.

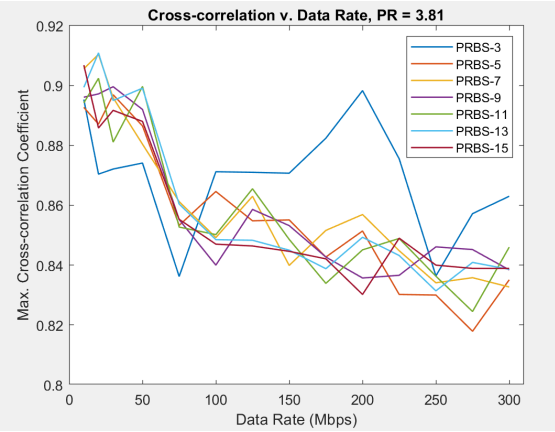

Figure 39. Cross-correlation v. data rate, PR = 3.81.

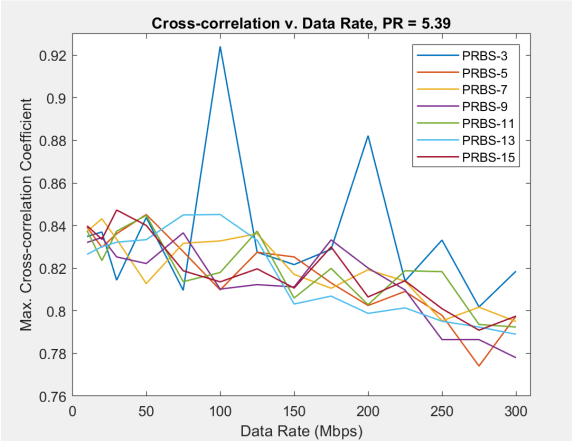

Figure 40. Cross-correlation v. data rate, PR = 5.39.

Conclusion and Future Work

Multiple-link free-space optical communication performance can be simulated, implemented, and evaluated using a testbed. Experimental results reported in this thesis detailed the feasibility of a testbed for obtaining real-time signal comparison, user detection, and cognitive switching. Threshold determination can be used accordingly to define system thresholds for any experimental setup. Real-time FastICA showed at least 0.89 cross-correlation, and direct subtraction showed at least 0.77 cross-correlation. Testing indicated that the proposed method can be used to isolate a signal from mixed sources.

In Chapter 2, only equal gain combining was used to combine channels to State 2. For future work, additional diversity schemes could be further investigated. For example, maximal ratio combining could be evaluated to further improve signal-to-noise ratio. With better equipment integration, number of users could be increased from two for all algorithms presented in this work. Because only OOK was used as optical modulation, it would be beneficial for other modulation schemes (e.g., OFDM and QAM) to be further examined.

References

[1] Free Space Optics (FSO) and Visible Light Communication (VLC)/Light Fidelity (Li-Fi) Market with COVID-19 Impact Analysis by Component (LED, Photodetector, Microcontroller, Software), Transmission Type, Application, Geography - Global Forecast to 2025

[2] M. Z. Chowdhury, M. T. Hossan, A. Islam and Y. M. Jang, "A Comparative Survey of Optical Wireless Technologies: Architectures and Applications," IEEE Access 6 (2018): 9819–40. https://doi.org/10.1109/ACCESS.2018.2792419.

[3] A Jahid, M. H. Alsharif, and T. J. Hall, "A Contemporary Survey on Free Space Optical Communication: Potential, Technical Challenges, Recent Advances and Research Direction," CoRR abs/2012.00155 (2020). https://arxiv.org/abs/2012.00155

[4] J. Li, M. Uysal, Achievable information rate for outdoor free space optical communication with intensity modulation and direct detection, in: Proceedings of the IEEE Global Telecommunications Conference (GLOBECOM) 2003, San Francisco, CA, Dec. 2003, pp. 2654–2658.

[5] F. Aveta, H. H. Refai and P. G. Lopresti, "Cognitive Multi-Point Free Space Optical Communication: Real-Time Users Discovery Using Unsupervised Machine Learning," in IEEE Access, vol. 8, pp. 207575-207588, 2020, doi: 10.1109/ACCESS.2020.3038624.

[6] J. C. Cartledge and A. S. Karar, "100 Gb/s Intensity Modulation and Direct Detection," in Journal of Lightwave Technology, vol. 32, no. 16, pp. 2809-2814, 15 Aug.15, 2014, doi: 10.1109/JLT.2014.2314611.

[7] K. Hedman and F. David, “Atmospheric refraction and its impact on free-space optic communication systems,” Nov. 2004, vol. 5572. doi: 10.1117/12.565475.

[8] A. Hyvarinen and E. Oja. 2000. "Independent Component Analysis: Algorithms and Applications." Neural Networks Research Centre, Helsinki University of Technology. Neural Networks 13, no. 4 (2000): 411–30. https://doi.org/10.1016/S0893-6080(00)00026-5.

[9] LabVIEW. 2010 TSA Independent Component Analysis VI. LabVIEW 2010 Advanced Signal Processing Toolkit Help.

Appendix A: Nomenclature

ASK	Amplitude-shift keying
BSS	Blind source separation
E/O	Electrical to optical converter
FSO	Free-space optics
FSOC	Free-space optics communication
GUI	Graphical user interface
ICA	Independent Component Analysis
IM/DD	Intensity modulation and direction detection
LOS	Line-of-sight
O/E	Optical to electrical converter
OFDM	Orthogonal frequency-division multiplexing
OOK	On-off keying
OWC	Optical wireless communication
PRBS	Pseudo-random binary sequence
PSK	Phase-shift keying
QAM	Quadrature amplitude modulation
QPSK	Quadrature phase-shift keying
RF	Radio frequency
SFP	Small form-factor pluggable
USBTMC	USB Test and Measurement class
V2X	Infrastructure-to-vehicle